RSC Advances

PAPER

View Article Online
View Journal | View Issue

Cite this: *RSC Adv.*, 2017, **7**, 47570

Promotional effect of niobium substitution on the low-temperature activity of a $WO_3/CeZrO_x$ monolithic catalyst for the selective catalytic reduction of NO_x with NH_3†

Haidi Xu,[a] Qingjin Lin,[b] Yun Wang,[c] Li Lan,[d] Shuang Liu,[a] Chenlu Lin,[a] Qin Wang,[c] Jianli Wang*[b] and Yaoiqng Chen *[ab]

A series of Nb-substituted $WO_3/CeZrO_x$ catalysts were prepared by the co-impregnation method and applied in the selective catalytic reduction of NO_x with NH_3 (NH_3-SCR). NH_3 oxidation, N_2 sorption, XRD, Raman, UV-vis, XPS, H_2-TPR, O_2/NH_3-TPD and *in situ* DRIFTS were performed to correlate the redox property and surface acidity to NH_3-SCR performance of Nb-substituted catalysts. The catalyst with 5 wt% substitution amount of Nb_2O_5 presented excellent deNO_x activity and N_2 selectivity in a broad reaction temperature window of 190–434 °C at a gas space velocity of 30 000 h^{-1}. The characterization results demonstrated that the partial substitution of WO_3 by Nb_2O_5 not only led to strong redox properties arising from abundant surface active oxygen species, but also promoted the adsorption of NH_3 and the redistribution of acid sites due to Nb–OH related to Brønsted acid sites and Nb=O bonded to strong Lewis acid sites. The enhancement of surface active oxygen species and Brønsted acid sites promoted the low-temperature (below 250 °C) deNO_x activity. However, the preoxidation of NH_3 at high temperatures slightly suppressed the NO_x conversion of the catalyst with more strong Lewis acid sites at above 400 °C. Moreover, the catalyst also showed excellent sulfur tolerance and could be a promising candidate for practical applications in NO_x abatement.

Received 31st July 2017
Accepted 30th September 2017

DOI: 10.1039/c7ra08429c

rsc.li/rsc-advances

1 Introduction

It is well known that nitrogen oxides (NO_x, including NO and NO_2) derived from stationary resources like the coal fired power plants and mobile resources like the diesel engine, as one of the main air pollutants, would lead to several severe environmental problems, such as haze, acid rain, greenhouse effect, ozone depletion and photochemical smog.[1,2] The emission regulations of many countries and regions are becoming more and more stringent, especially in the United States, Europe, Japan and China, in order to cope with serious pollution impacts of NO_x.[3,4] Currently, among the proposed or developed various techniques for NO_x abatement, the selective catalytic reduction of NO_x with NH_3 (NH_3-SCR) as a reductant is the most effective technology to remove NO_x and has been widely used in the oxygen-rich exhausts.[2,3] Until now, V_2O_5/WO_3 (MoO_3)/TiO_2 serial catalyst is still the most typical commercial and well-studied metal oxides catalyst, even though it still has some drawbacks to solve, such as narrow operation temperature range, low N_2 selectivity, low thermal stability due to the phase transformation of TiO_2 from anatase to rutile at the high temperature range and the volatility and toxicity of vanadium oxide species.[5,6] As a result, it is necessary to develop novel environmental friendly metal oxide NH_3-SCR catalyst which possesses excellent low-temperature deNO_x activity, high N_2 selectivity and strong thermal stability in a broad operation temperature window, to be a promising candidate to substitute the conventional V-based catalysts.

In recent, increasing interests have been focused on the cerium-based NH_3-SCR catalysts and ceria zirconia mixed oxides could be one of the most promising supports for NO_x abatement, considering its acid–base property, redox property and thermal stability.[7,8] Among them, WO_3/CeO_2–ZrO_2 serial catalysts have received increasing attentions since reported by Li *et al.*[9] It was reported that NO_x could be completely converted over WO_3/CeO_2–ZrO_2 in a broad temperature range of 200–

[a]*Institute of New Energy and Low-Carbon Technology, Sichuan University, Chengdu 610064, PR China. E-mail: nic7501@scu.edu.cn; Fax: +86-28-85418451; Tel: +86-28-85418451*

[b]*College of Chemistry, Sichuan University, Chengdu 610064, PR China. E-mail: wangjianli@scu.edu.cn; Fax: +86-28-85418451; Tel: +86-28-85418451*

[c]*Sinocat Environmental Technology Co., Ltd, Chengdu 611731, PR China*

[d]*College of Pharmacy and Biological Engineering, Chengdu University, Chengdu 610106, PR China*

† Electronic supplementary information (ESI) available: The N_2 selectivity of 10W/CZ, Nb-substituted W/CZ and 10Nb/CZ, sulfur tolerance of 5W–5Nb/CZ, H_2-TPR profiles after deconvolution of 10W/CZ 5W–5Nb/CZ and 10Nb/CZ. See DOI: 10.1039/c7ra08429c

500 °C with the condition of $NO/NO_2 = 1:1$, the catalyst presented higher thermal stability than conventional V_2O_5–WO_3–TiO_2. After that, the promotion of WO_3/CeO_2–ZrO_2 has been investigated to improve its NH_3-SCR performance and seek its NH_3-SCR reaction mechanism by different methods. For example, Zhang *et al.*[10] used different synthesis methods to modify the morphology of CeO_2–ZrO_2–WO_3 and achieve the optimal NH_3-SCR performance; Can *et al.*[11] altered the molar ratio of Ce/Zr and investigated its impact on a NO_x storage reduction–selective reduction coupled process; Väliheikki *et al.*[12] studied the impact of SO_2 and hydrothermal aging on the NH_3-SCR activity of W–CeZr catalyst. Our group has investigated the influences of molar ratios of Ce/Zr and W/Fe on the NH_3-SCR performance of $FeW/Ce_xZr_{1-x}O_2$, respectively, and found that $FeW_{1.03}/Ce_{0.68}Zr_{0.32}O_2$ (Ce/Zr = 68/32 and W/Fe = 1.03) could achieve the highest NO_x conversion (higher than 95% NO_x conversion in the range of 250–435 °C) under our test conditions.[13,14] And then, the effects of the calcination temperature of CZ on the structure and NH_3-SCR performance of $WO_3/Ce_{0.68}Zr_{0.32}O_2$ (denoted as W/CZ) were investigated and the catalyst calcined at 500–600 °C with higher thermal stability was obtained.[15] In order to improve the sulfur tolerance of W/CZ, different loadings of TiO_2 were introduced into CZ by a co-precipitation method and used to prepare $WO_3/CeZrTi_xO_2$ (W/CZT*x*) for NH_3-SCR, respectively.[16] It was found that the addition of TiO_2 not only improved the sulfur tolerance but also enhanced the NO_x conversion of W/CZ, the operation temperature window (the temperature range in which higher than 90% NO_x conversion was achieved) of W/CZT20 with 20 wt% TiO_2 was widened to 200–470 °C from 224–444 °C of W/CZ.

However, it is inevitable that TiO_2 would easily transform from anatase to rutile even though with low loading of TiO_2, when the catalyst encountered the regeneration of diesel particulate filters (DPF) equipped in the upstream of NH_3-SCR catalyst.[17] Therefore, it is imperative to search one component introduced into W/CZ to develop a novel modified W/CZ catalyst without titanium, but the catalyst should keep the strong sulfur tolerance and excellent low-temperature catalytic activity of W/CZT20. Recently, NbO_x has attracted much attention as a promoter to improve the NH_3-SCR performance due to its unique acid property as well as excellent redox property.[18–20] Usually, Nb_2O_5 was introduced into CeO_2-based catalysts, which could not only promote the acidity of catalysts but also modify the redox property by generating oxygen vacancies due to the electronic interaction between Ce^{n+} and Nb^{n+}, to achieve better NH_3-SCR performance.[19,21,22] Ding *et al.* and Casapu *et al.* reported that the Nb_2O_5 modified $CeZrO_2$ catalyst presented high $deNO_x$ activity and N_2 selectivity, strong sulfur/water vapor resistance and hydrothermal stability.[22,23]

Therefore, in this work, a series of Nb-substituted W/CZ catalysts were prepared by co-impregnation method and applied for NO_x removal by NH_3-SCR reaction. The obtained 5W–5Nb/CZ catalyst with 5 wt% WO_3 substituted by Nb_2O_5 exhibited better NH_3-SCR activity than W/CZT20 in the previous work and maintained the sulfur tolerance of the latter. Several characterizations on the structure, redox property and surface acidity of Nb-substituted W/CZ catalysts were employed to illustrate the effects of Nb substitution on the catalytic performance of catalysts.

2 Experimental

2.1 Catalysts preparation

The carrier material $CeZrO_2$ mixed oxides (denoted as CZ) were prepared by the conventional co-precipitation method followed as our previous work.[15] Different amounts of Nb_2O_5 substituted $WO_3/CeZrO_2$ (labeled as W/CZ) catalysts were prepared by co-impregnating the asprepared CZ powders calcined at 600 °C for 3 h with ammonium metatungstate hydrate ($(NH_4)_6H_2W_{12}O_{40}$, AR grade, 99.9%, Anda, China) and nibium(v) oxalate hydrate ($C_{10}H_5NbO_{20}$, AR grade, 99.9%, Alfa Aesar, China) mixed solution. The total loadings of WO_3 and Nb_2O_5 were 10 wt%, the mass ratios of WO_3/Nb_2O_5 were 10 : 0, 7 : 3, 5 : 5, 3 : 7 and 0 : 10, respectively. The impregnated powders were dried at 120 °C overnight, and then calcined at 550 °C for 3 h in air. The resulting five catalyst powders were subsequently coated on honeycomb cordierites (cylinder, radius: 5.5 mm, length: 26 mm, bulk: 2.5 mL, 62 cell per cm^{-2}, Coring, USA), and then dried at 120 °C overnight and calcined at 550 °C for 3 h in air. Finally, Nb-substituted W/CZ monolithic catalysts with coating amount of about 160 g L^{-1} were obtained and separately denoted as 10W/CZ, 7W–3Nb/CZ, 5W–5Nb/CZ, 3W–7Nb/CZ and 10Nb/CZ.

2.2 Catalytic activity measurements

The NH_3-SCR activity measurements of the prepared monolithic catalysts were carried out in a fixed-bed quartz tube flow reactor at atmospheric pressure. The flue gas composition was as follows: 500 ppm NO (when used), 500 ppm NH_3 (when used), 5% O_2, N_2 as balance. The experimental procedures of water steam, sulphur and carbon dioxide were employed to 100 ppm SO_2 (when used), 10 vol% water vapour, 10% CO_2 and their mixtures into the above reaction gas. The premixed gases (2.0% NO in N_2, 2.0% NH_3 in N_2, 0.1% SO_2 in N_2, 99.99% CO_2 and 99.99% O_2) were supplied by Testing Technology Research Institute, China. Reactant gases were regulated by mass-flow controllers before entering the reactor. In typical condition, 2.5 cm^3 monolithic catalyst sample was used in each run and the total flow rate was about 1.25 L min^{-1}, yielding the GHSV of 30 000 h^{-1} by volume. The separate NH_3/NO oxidation activity was tested in the absence of NO/NH_3. The concentrations of NH_3, NO_x and N_2O in the inlet and outlet gases were continually analyzed by an FT-IR (Antaris IGS, Nicolet). The data were recorded after 30 min when the reaction reached a steady state for each test.

The NO_x conversions (X_{NO_x}) and N_2 selectivity (S_{N_2}) were calculated as follows:

$$X_{NO_x}\ (\%) = \frac{C_{in} - C_{out}}{C_{in}} \times 100 \quad (1)$$

$$S_{N_2}\ (\%) = \left(1 - \frac{2[N_2O]_{out}}{([NO_x]_{in} - [NO_x]_{out}) + ([NH_3]_{in} - [NH_3]_{out})}\right) \times 100 \quad (2)$$

where, $[NO_x] = [NO] + [NO_2]$, C_{in} and C_{out} denoted the inlet and outlet gas concentration of NO_x, respectively.

2.3 Characterizations

The textural properties of all catalysts were measured by N_2 adsorption–desorption at −196 °C on a Quantachrome automated surface area & pore size analyzer (Autosorb SI). The samples were pretreated at 300 °C for 3 h prior to the measurement. The surface areas were determined by Brunauer–Emmett–Teller (BET) model.

Powder X-ray diffraction (XRD) patterns of samples were collected in the 2θ range of 10–80° using a Rigaku D/max-RA Diffractometer equipped with a Cu K_α ($\lambda = 0.15406$ nm) radiation resource operated at 40 kV and 100 mA, respectively.

Visible Raman spectra of all catalysts were collected on a Lab-RAM HR laser Raman spectrograph with a spectral resolution of 2 cm^{-1} at room temperature. A Nd:Yag laser of 532 nm was used as the excitation source with a power output of 30 mW. All specimens were illuminated through a 50× objective and in powder form to prevent diffusion problems. Raman spectra were collected and recorded over the spectral range of 100–1000 cm^{-1}. The specification of the grating was 600 g mm^{-1}.

The UV-vis spectra (UV-vis) were performed in diffuse reflectance mode using PerkinElmer Lambda 750S spectrometer (USA) equipped with an internal integration sphere. The test samples were the mixture of the catalyst powder and $BaSO_4$ with the weight ratio of 1 : 6. The spectra were collected in the spectra range of 200–800 nm at room temperature.

The X-ray photoelectron spectra (XPS) data were recorded on Thermo Escalab 250Xi electron spectrophotometer with 15 kV high pressure and 14.9 mA electric current using Al K_α radiation (1486.6 eV), and operating in a constant pass energy mode (20 eV pass energy). The C 1s peak at 284.6 eV was used for the calibration of binding energy values. And the semi-quantitative surface relative atomic concentrations were obtained from the eqn (3). The pressure in the analytical chamber was about 10^{-8} Pa.

$$\frac{n_i}{n_j} = \frac{I_i}{I_j} \times \frac{\sigma_j}{\sigma_i} \times \frac{{E_{k_j}}^{0.5}}{{E_{k_i}}^{0.5}} \quad (3)$$

n: surface atomic concentration; I: intensity or area of the XPS peak. σ: the photo-ionization cross-section of the corresponding energy level of the element, using Scofield data; E_k: the kinetic energy of photoelectron, $E_k = h\nu$ − B.E. (Al Kα, $h\nu = 1486.6$ eV); i and j: the corresponding element of samples.

Temperature programmed reduction of H_2 (H_2-TPR) experiments were performed in TP-5076 (Xianquan, Tianjin, China) with a thermal conductivity detector. All catalysts (100 mg) were pretreated in a quartz tubular micro-reactor in a flow of N_2 at 450 °C for 1 h to yield a clean surface, and then cooled down to room temperature. The reduction was carried out in a flow of 5 vol% H_2–95 vol% N_2 to 800 °C with a heating rate of 10 °C min^{-1}.

O_2/NH_3-TPD experiments were carried out in TP-5076 (Xianquan, Tianjin, China) with a thermal conductivity detector. A typical sample mass of 100 mg and a gas flow rate of 30 mL min^{-1} were used during the experiments. The experiment included four stages: (1) degasification of the sample in N_2 at 400 °C for 1 h to clear the surface, (2) adsorption of 2 vol% NH_3/O_2–98% N_2 at 80 °C for 1 h, (3) isothermal desorption in N_2 at 80 °C until no NH_3/O_2 was detected and (4) temperature programmed desorption in N_2 at 10 °C min^{-1} up to 900 °C. The detector was a thermal conductivity detector.

The *in situ* diffuse-reflectance infrared Fourier transform spectroscopy (*in situ* DRIFTS) of adsorbed species arising from NH_3 adsorption at various temperature over the catalysts, were collected in the range of 4000–1000 cm^{-1} using Thermo Nicolet 6700 FTIR spectrometer. Diffuse reflectance measurements were performed *in situ* in a high temperature cell equipped with a KBr window. The catalyst was heated to 350 °C under N_2 at a total flow rate of 100 mL min^{-1} for 1 h to remove any adsorbed impurities. And then the catalyst was cooled down to 50 °C, exposed to 1000 ppm NH_3/N_2 (100 mL min^{-1}) for 1 h, and subsequently flushed with N_2. Afterwards, the DRIFTS spectra of catalysts were collected between 50 and 300 °C at a 50 °C interval. The background spectrum was collected once every 50 °C in flowing N_2 during the cooling process.

3 Results and discussions

3.1 Catalytic performance

3.1.1 NH_3-SCR activity. Fig. 1a showed the NH_3-SCR activity over 10W/CZ, Nb-substituted W/CZ and 10Nb/CZ catalysts. NO_x could be completely reduced in the temperature range of 222–450 °C over 10W/CZ. From the results of NO_x conversion in Fig. 1a, it can be seen that the partial substitution of WO_3 with Nb_2O_5 could indeed affect the deNO_x activity of 10W/CZ, the NO_x conversion had an obvious increase in the relatively low temperature range. When 5 wt% WO_3 was substituted by Nb_2O_5, 5W–5Nb/CZ showed the best activity, over which the light-off temperature (T_{50}, at which 50% NO_x was converted) and the complete conversion temperature (T_{90}, at which higher than 90% NO_x was achieved) of NO_x was lowered to 160 °C (from 180 °C of W/CZ) and 190 °C, respectively, which was better than WO_3/CeZrTiO_x (denoted as W/CZT20, T_{50} = 170 °C and T_{90} = 200 °C) in our previous work.[16] However, the continuing substitution of WO_3 by more Nb_2O_5 resulted in the decrease of the deNO_x activity, and the T_{90}s of 3W–7Nb/CZ and 10Nb/CZ were both shifted to about 215 °C, which was slightly lower than that of 10W/CZ. The apparent low-temperature NH_3-SCR activity was enhanced in the following sequence: 10W/CZ < 10Nb/CZ ≈ 3W–7Nb/CZ < 7W–3Nb/CZ < 5W–5Nb/CZ. It should be noted that the substitution of WO_3 by Nb_2O_5 could dramatically decrease the high-temperature NO_x conversion in Fig. 1a. For example, T_{90}s of catalysts at the high-temperature range were shifted to relatively lower temperature in the following order: 10 W/CZ (450 °C) > 7W–3Nb/CZ (434 °C) ≈ 5W–5Nb/CZ (434 °C) > 3W–7Nb/CZ (405 °C) > 10Nb/CZ (389 °C). In

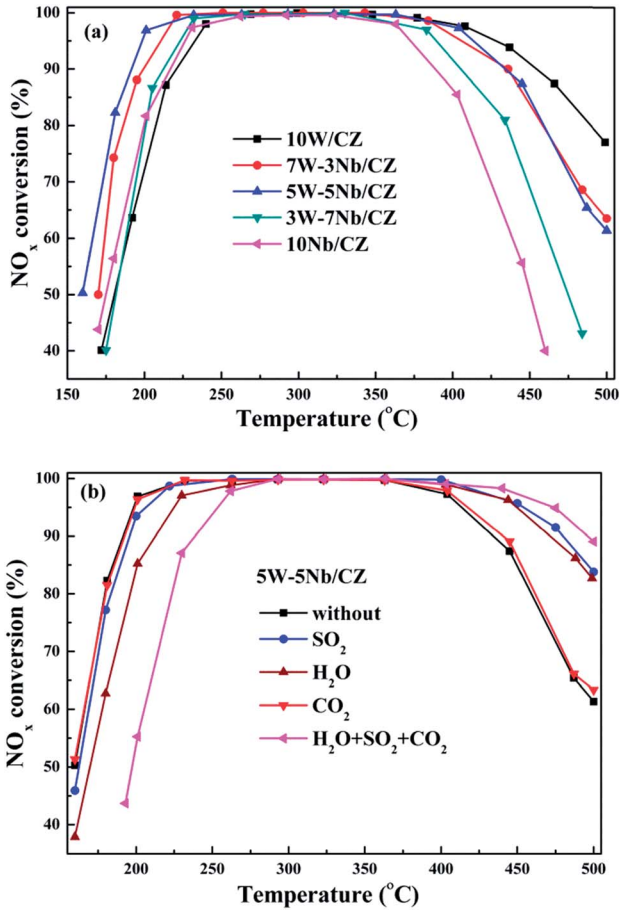

Fig. 1 NO_x conversion of 10W/CZ and Nb-substituted W/CZ and 10Nb/CZ catalysts (a) and the effects of H_2O, SO_2 and CO_2 on NO_x conversion over 5W–5Nb/CZ catalysts (b). Reaction conditions: 500 ppm NO, 500 ppm NH_3, 5% O_2, 100 ppm SO_2 (when used), 10 vol% H_2O (when used), 10% CO_2 (when used) and N_2 as balance gas, the total gas rate: 1.25 L min^{-1}, GHSV: 30 000 h^{-1}.

previous work done by Wu's group,[19] they also observed that more Nb_2O_5 could lead to the depress of NO_x conversion both in low and high-temperature ranges. The decrease of the high-temperature activity could be resulted from extra NO_x generated from non-selective oxidation of NH_3 at high-temperature ranges. Moreover, Fig. S1† presented the N_2 selectivity and the amount of N_2O formed in NH_3-SCR reaction over the catalysts. The N_2 selectivity of all investigated catalysts was slightly decreased with the increase of the operation temperature, but 10W/CZ still had higher than 97% of the minimum N_2 selectivity and the Nb-containing catalysts possessed higher than 98% N_2 selectivity at their corresponding highest testing temperatures. It was clearly that the amount of Nb_2O_5 substitution was a key factor to achieve high NH_3-SCR activity and hardly influenced the N_2 selectivity.

W/CZT20 catalyst presented excellent sulfur tolerance in our previous work.[16] In order to compare the sulfur tolerance of 5W–5Nb/CZ and W/CZT20, 100 ppm SO_2 was injected into the reaction gas and the NH_3-SCR activities of the two catalysts in the temperature range of 160–500 °C were shown in Fig. S2.† It was clear that 5W–5Nb/CZ still presented high NO_x conversion in the presence of SO_2 from Fig. 1b. The low-temperature (below 220 °C) NO_x conversion of 5W–5Nb/CZ was slightly affected by the introduction of SO_2, its T_{50} and T_{90} were shifted to 162 °C from 160 °C and 190 °C to 195 °C, respectively. Furthermore, the deNO_x activity of the catalyst was evidently improved by the presence of SO_2 at above 400 °C, its T_{90} at high temperature range was transferred to 480 °C from 434 °C. Similar as W/CZT20, the influence of SO_2 on the NO_x conversion over 5W–5Nb/CZ was negligible in the low-temperature range. However, the NH_3-SCR activities of 5W–5Nb/CZ in the absence or presence of SO_2 were both higher than the corresponding catalytic activity of W/CZT20. Moreover, water steam, SO_2 and CO_2 often coexist in the exhausted gas emitted from the diesel engine. The co-effect of H_2O, SO_2 and CO_2 on the NH_3-SCR activity over 5W–5Nb/CZ was investigated in this work, and the results were displayed in Fig. 1b. The influence of CO_2 on the NO_x conversion of the catalyst could be neglected from Fig. 1b. But the effect of H_2O on low-temperature activity was more negative than single SO_2 or CO_2, the T_{50} and T_{90} were transferred from 160 °C to 170 °C and 190° to 212 °C, respectively. The above phenomenon could be ascribed to H_2O with stronger adsorption ability than SO_2 and CO_2 at the low-temperatures.[2] As seen from Fig. 1b, the co-presence of H_2O, SO_2 and CO_2 further depressed the low-temperature NO_x conversion compared with the separate component. Nevertheless, the catalyst still could achieve higher 90% NO_x conversion in the temperature range of 235–495 °C. Thus, 5W–5Nb/CZ showed excellent tolerances of water steam, sulfur and carbon dioxides, which could make it to be a promising catalyst of NO_x abatement for practical application.

3.1.2 NO oxidation. It was well known that the presence of NO_2 usually played a promotional role in the low-temperature NH_3-SCR reaction over the metal oxides catalysts, owing to the "Fast SCR" reaction ($NO + NO_2 + 2NH_3 \rightarrow 2N_2 + 3H_2O$) as the rate-controlled step rather than the "Standard SCR" reaction ($4NO + 4NH_3 + O_2 \rightarrow 4N_2 + 6H_2O$) in the low-temperature range.[24] The activity of NO oxidized to NO_2 was tested over 10W/CZ, 5W–5Nb/CZ and 10Nb/CZ catalysts and the results were displayed in Fig. 2. It could be seen that the activity of NO oxidation below 300 °C was increased in the followed sequences: 10W/CZ < 10Nb/CZ < 5W–5Nb/CZ, as shown in Fig. 2. It meant that Nb partial substituted catalyst presented higher NO oxidation activity than 10W/CZ and 10Nb/CZ at low temperatures, although more NO_2 was generated over the latter rather than 5W–5Nb/CZ above 325 °C. The above results were in line with the NH_3-SCR activity in Fig. 1a, which indicated that 5W–5Nb/CZ possessed higher NO_x conversion in the low-temperature range than other catalysts due to more NO_2 taking part in the "Fast SCR" reaction over the former.

3.1.3 NH_3 oxidation. The separate NH_3 oxidation experiments were carried out and the results were displayed in Fig. 3. It could be found that the activity of NH_3 oxidation of 10W/CZ was evidently higher than those of the Nb-containing catalysts and 5W–5Nb/CZ showed the highest NH_3 conversion in Fig. 3a. It suggested that the oxidation ability of 5W–5Nb/CZ was obviously promoted by partial substitution of WO_3 with Nb_2O_5. Additionally, it should be noted in Fig. 3b and c that the

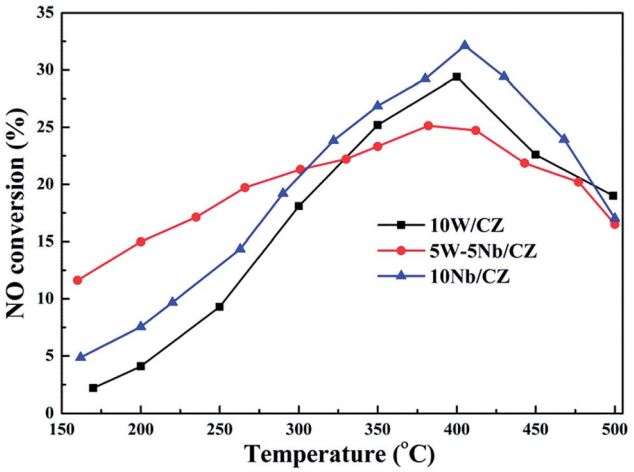

Fig. 2 Separated NO oxidation activity over 10W/CZ, 5W–5Nb/CZ and 10Nb/CZ. Reaction conditions: 500 ppm NO, 5% O_2, N_2 balance, the total gas rate: 1.25 L min^{-1}, GHSV: 30 000 h^{-1}.

generated amounts of NO and NO_2 over 10Nb/CZ were evidently higher than those over other two catalysts, suggesting that the existence of Nb_2O_5 was beneficial to the non-selective oxidation of NH_3 to form NO and NO_2 and finally led to the decrease of NO_x conversion in the high-temperature range. Although the amounts of NO and NO_2 over 5W–5Nb/CZ were still higher than those over 10W/CZ, compared to 10Nb/CZ, the concentrations of NO_x were dramatically depressed. It implied that the peroxidation of NH_3 was inhibited due to the partial substitution of WO_3 by Nb_2O_5 over 5W–5Nb/CZ even with stronger oxidation ability than 10Nb/CZ. These phenomena could directly illustrate that the decline of the high-temperature NH_3-SCR activity (in Fig. 1a) over the Nb-containing catalysts derived from the non-selective oxidation and peroxidation of NH_3. Moreover, less than 5 ppm N_2O was formed in the NH_3 oxidation reaction over the three investigated catalysts from Fig. 3d.

3.2 Textural and structural properties

3.2.1 N_2 sorption and XRD. The N_2 sorption isotherms of the five catalysts indicated that the partial substitution of WO_3 by Nb_2O_5 could not change the type of the isotherm of 10W/CZ, which were not shown in here. Textural properties, including surface area, cumulative pore volume and average pore radius, were summarized in Table 1, which suggested that the Nb substitution slightly affected the textural properties of 10W/CZ. Although the surface area and pore volume of 5W–5Nb/CZ were higher than those of other catalysts, the differences among them could be in the range of error. Therefore, the textural properties could not be the main reasons that affected NH_3-SCR activity in this work.

Powder XRD was employed to investigate the effect of the substitution of WO_3 by Nb_2O_5 on the crystal structure of 10W/CZ, and the XRD patterns were presented in Fig. 4. The typical diffraction peaks located at around 28.9° observed over all catalysts were ascribed to the cubic $Ce_{0.75}Zr_{0.25}O_2$ phase (JCPDS 28-0271). And the intensities of the $Ce_{0.75}Zr_{0.25}O_2$ diffraction

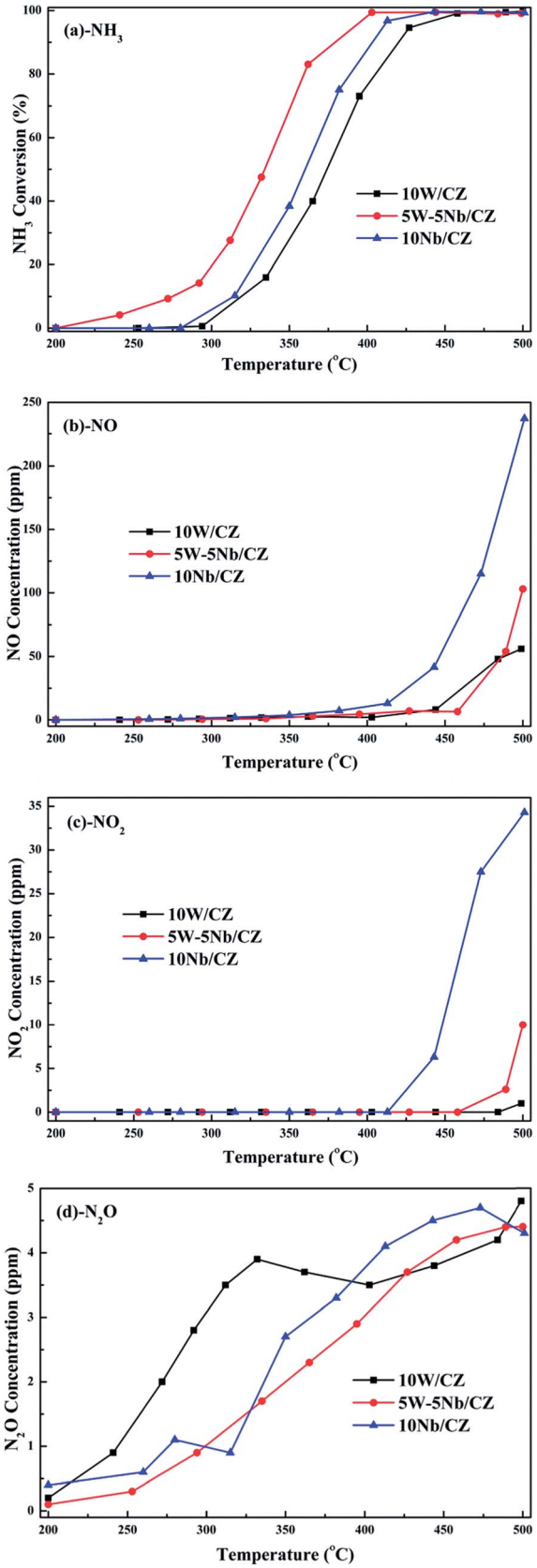

Fig. 3 Separated NH_3 oxidation activity (a), the concentrations of formed NO (b), NO_2 (c) and N_2O (d) over 10W/CZ, 5W–5Nb/CZ and 10Nb/CZ. Reaction conditions: 500 ppm NH_3 (when used), 5% O_2, N_2 as balance, total flow rate: 1250 mL min^{-1}, GHSV: 30 000 h^{-1}.

Table 1 Textural and structural properties of catalysts

Samples	Surface area ($m^2\ g^{-1}$)	Pore volume ($cm^3\ g^{-1}$)	Pore radius (nm)	2θ (°)	Lattice parameter (nm)	Crystal size (nm)
10W/CZ	98.9	0.242	4.90	28.880	0.5347	6.0
7W–3Nb/CZ	97.1	0.236	4.86	28.980	0.5333	5.8
5W–5Nb/CZ	102.5	0.241	4.70	28.940	0.5335	5.8
3W–7Nb/CZ	97.0	0.221	4.56	28.840	0.5337	5.8
10Nb/CZ	104.8	0.242	4.61	28.780	0.5336	5.7

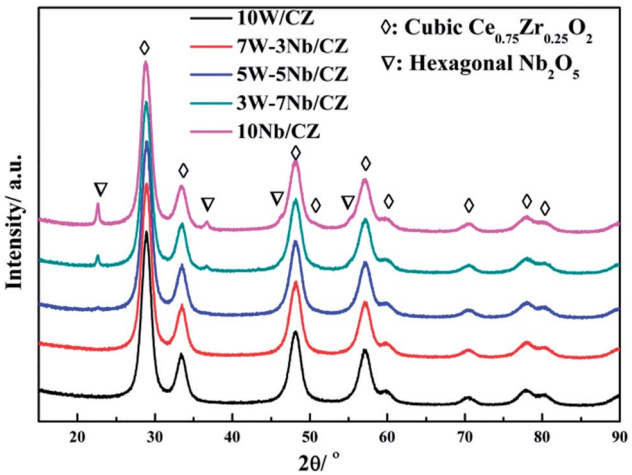

Fig. 4 XRD images of the catalysts.

peaks could not be depressed by Nb_2O_5 substitution. When the substitution amount was 3 wt%, the lattice parameter was evidently decreased and the 2θ of the main diffraction peak was shifted to higher value compared to those of 10W/CZ in Table 1. Moreover, no typical diffraction peaks ascribed to Nb_2O_5 crystallites were observed over 7W–3Nb/CZ in Fig. 3. It indicated that the incorporation of Nb into the lattice of $Ce_{0.75}Zr_{0.25}O_2$ could lead to a shrinkage of the crystal cells due to that the radius of Nb^{5+} (0.070 nm) was smaller than those of Ce^{4+} (0.092 nm) and Zr^{4+} (0.080 nm).[16] Further enhanced the substitution amount of Nb_2O_5, a very weak diffraction peak ascribed to the hexagonal Nb_2O_5 (JCPDS 28-0317) phase located at around 22.4° was found over 5W–5Nb/CZ. Further increasing the amount of Nb_2O_5, the intensities of the hexagonal Nb_2O_5 phases were gradually enhanced, the values of 2θ were slightly transferred to lower ranges, but there was no obvious difference among the lattice parameters of the Nb-containing catalysts. The above facts suggested that more Nb_2O_5 could not incorporate into the lattice of $Ce_{0.75}Zr_{0.25}O_2$ and disperse on the surface of the CZ carrier when the substitution amount of Nb_2O_5 was higher than 5 wt%, because other diffraction peaks ascribed to the hexagonal Nb_2O_5 at around 36.7, 46.2, 50.7 and 55.2° could be observed over 3W–7Nb/CZ and 10Nb/CZ rather than 5W–5Nb/CZ.

3.2.2 Raman. Normalized Raman spectroscopy, as an effective characterization technique, was carried out on 10W/CZ, Nb-substituted W/CZ and 10Nb/CZ, to achieve detailed information about the fine structures of catalysts. The results were displayed in Fig. 5. An intense band at *ca.* 465 cm^{-1} was corresponded to the typical Raman spectra of cerium zirconium solid solution due to the F_{2g} vibration mode of the cubic fluorite structure, which could be viewed as the symmetric breathing vibrational mode of the oxygen anions and cerium cations.[15,19,21] Nanoparticle size could change the Raman band position and the linewidth of the 456 cm^{-1} peak.[25] As seen from Table 1, the crystallize sizes of all catalysts were around 6 nm, suggesting that the crystallize size was similar as the grain size in the nano-size range. From Fig. 5, the linewidth of F_{2g} Raman band (465 cm^{-1}) slightly decreased with the enhancement of the substituted amount of Nb_2O_5, which was ascribed to the grain growth and related with the XRD results.[26] The normal Raman inactive transverse and longitudinal optical phonon modes were detected at *ca.* 300 and 618 cm^{-1} over all catalysts, respectively, which was closely related to the substitution of the oxygen atoms on the ideal fluorite structure, resulting in the transformation of the ideal fluorite structure.[19,27] It could be seen that the intensities of the two bands slightly increased with the improvement of the partial substitution of WO_3 by Nb_2O_5. Among them, 5W–5Nb/CZ with higher intensities of these bands than other catalysts was beneficial to form more oxygen vacancies. In addition, a broad band located at *ca.* 820 cm^{-1} was firstly observed on 5W–5Nb/CZ, which was attributed to the monomeric NbO_x species with tetrahedral [NbO_4] structure.[18,28] Meanwhile, a weak band at *ca.* 870 cm^{-1} ascribed to polymeric niobium oxide species with octahedral [NbO_6] with terminal

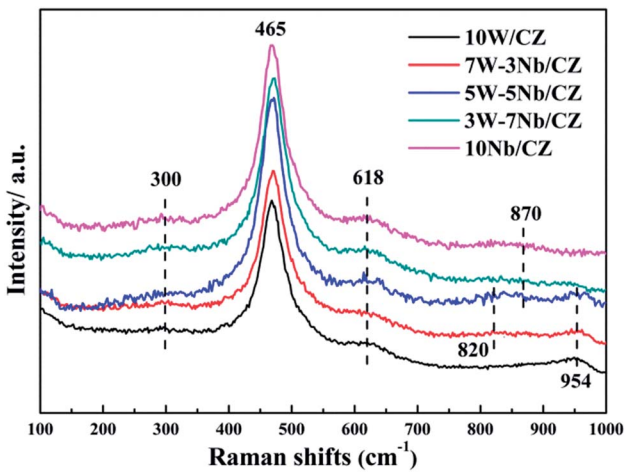

Fig. 5 Raman spectra of 10W/CZ, Nb-substituted W/CZ and 10Nb/CZ-700 catalysts.

Nb=O bonds was also emerged on 5W–5Nb/CZ.[19] Additionally, its intensity was further increased when the loading of Nb_2O_5 was enhanced to 10 wt%, indicating a decline in the ratio of monomeric NbO_x species and an the enhancement in degree of polymerization of surface NbO_x species at high Nb_2O_5 loading.[29] The above phenomena were consistent with the XRD results, a very weak peak assigned to Nb_2O_5 species was detected over 5W–5Nb/CZ and the peak intensity was increased with enhancing the loading of niobium to 10 wt%. It also illustrated a decrease in the dispersion of Nb_2O_5 species from the XRD results, when the content of Nb_2O_5 was higher than 5 wt%. According to the ref. 19, monolayer NbO_x structured with $[NbO_4]$ would be easier to contact the surface of CZ carrier and improve the amount of Brønsted and strong Lewis acid sites, thus, 5W–5Nb/CZ could possess larger amount of Brønsted and strong Lewis acid sites than other catalysts. Furthermore, a broad weak peak centered at *ca.* 954 cm^{-1} could be assigned to the $[WO_4]$ or $[WO_6]$ units (amorphous WO_x species) with symmetrical W=O stretching mode,[30,31] which could be detected over all W-containing catalysts, except for 3W–7Nb/CZ and 10Nb/CZ. There were no obvious differences among their intensities of the bands for the three catalysts, implying that the dispersion of tungsten oxides species could not be changed by the substitution of Nb_2O_5.

3.2.3 UV-vis. Table 2 summarized the adsorption edges and band gap widths of the five catalysts calculated according to the UV-vis spectra, and the corresponding UV-vis spectra were presented in Fig. 6. All catalysts showed an absorption edge ascribed to the O_{2p}–Ce_{4f} ligand–metal charge transfer in the visible range of 487–504 nm.[32] For 10W/CZ and 10Nb/CZ, the adsorption edges were estimated to be approximately 487.3 and 489.5 nm, and their corresponding band gap width were about 2.54 and 2.53 eV, respectively. As displayed in Fig. 6 and Table 2, the above two adsorption edges were both smaller than those of the catalysts in which WO_3 was partially substituted by Nb_2O_5. Moreover, compared with 10W/CZ, the adsorption edge was shifted to higher wavelengths with increasing substitution amount of Nb_2O_5, which illustrated that the electronic interaction existed between cerium and niobium in W–Nb/CZ catalysts and was affected by the substitution amount of Nb_2O_5.[19] Among them, 5W–5Nb/CZ possessed the strongest electronic interaction among the five investigated catalysts. According to the references, the adsorption edge of the CeO_2 containing Ce^{3+} in the CeO_2 lattice was about 650 nm, the partial reduction of Ce^{4+} to Ce^{3+} could result in the red shift of the adsorption edge and enhance the amount of Ce^{3+}.[19,33] Combined Fig. 5 and Table 2, it could be seen that the red shift of the absorption edge and the depress of the band gap width may lead to an increased ratio of Ce^{3+}/Ce in W–Nb/CZ, therefore, it was plausible to possess the largest amount of Ce^{3+} in 5W–5Nb/CZ.

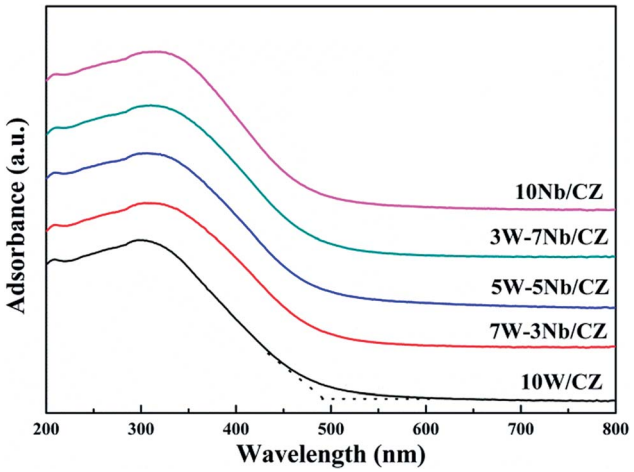

Fig. 6 UV-vis spectra of the catalysts.

3.2.4 XPS. To better understand the surface components and chemical states of different elements over the surface of catalysts, the selected 10W/CZ, 5W–5Nb and 10Nb/CZ catalysts were characterized *via* XPS technique. The XPS spectra of Ce 3d, O 1s and Nb 3d were displayed in Fig. 7a–c, respectively, and the surface atomic concentrations of all elements in catalysts were listed in Table 3. The spectra of Ce 3d were deconvoluted to two series of spin orbital multiplets by Gaussian–Lorentz fitting procedure, denoted as v and u. Thus, the molar ratio of Ce^{3+} in Ce on the surface of each catalyst was calculated by referred the previous work.[16] As listed in Fig. 7a and Table 3, the calculated atomic ratios of Ce^{3+}/Ce were according to the following sequence: 10W/CZ (20.9%) < 10Nb/CZ (25.09%) < 5W–5Nb/CZ (30.53%). The above results indicated that the partial substitution of WO_3 by Nb_2O_5 could obviously enhance the surface amount of Ce^{3+} over the catalyst, which was in agreement with the results of UV-vis. The incorporation of Nb^{5+} into the lattice of CZ to substitute Ce^{4+} or Zr^{4+} from the results of XRD, due to the smaller radius of Nb^{5+} (0.070 nm) than those of Ce^{4+} (0.092 nm) and Zr^{4+} (0.080 nm), resulted in the presence of excess electrons, which could be balanced by the formation of Ce^{3+}.[19]

As presented in Fig. 7b, two bands attributed to different oxygen species were obtained after fitting the spectra of O 1s. The first band at *ca.* 529.2 eV could be ascribed to the lattice oxygen, labeled as O_α, and the additional band at *ca.* 531.2 eV was assigned to the chemisorbed oxygen, denoted as O_β.[16,34] The relative ratios of O_β in O on the surface of the catalysts were quantified by the following formula: O_β = area (O_β)/[area (O_α) + area (O_β)] and shown in Fig. 7b. The value of 5W–5Nb/CZ was much higher than those of 10W/CZ and 10Nb/CZ, which was consistent with the above Ce^{3+}/Ce ratio. In other words, the partial substitution of WO_3 by Nb_2O_5 could form more

Table 2 Adsorption edges and band gap widths of different catalysts calculated from UV-vis spectra

Sample	10W/CZ	7W–3Nb/CZ	5W–5Nb/CZ	3W–7Nb/CZ	10Nb/CZ
Adsorption edge (nm)	487.3	499.1	503.7	491.1	489.5
Band gap width (eV)	2.54	2.48	2.46	2.52	2.53

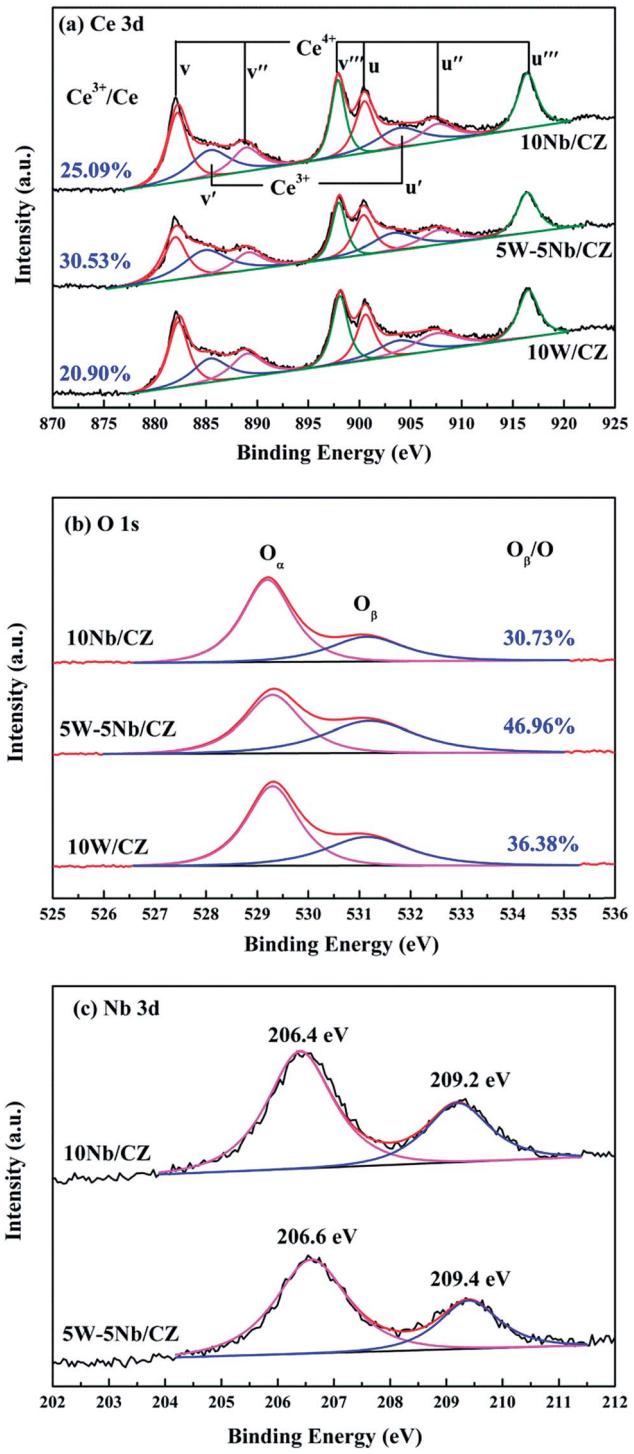

Fig. 7 XPS spectra of Ce 3d, O 1s and Nb 3d for 10W/CZ, 5W–5Nb/CZ and 10Nb/CZ catalysts.

chemisorbed oxygen accompanied with more Ce^{3+} on the surface of 5W–5Nb/CZ, as indicated by the Raman results. It could be contributed to that more Ce^{3+} resulted in more charge imbalance and unsaturated chemical bonds, which was beneficial for generating more oxygen vacancies and active oxygen.[15] Li *et al.*[21] and Weng *et al.*[35] suggested that Nb could activate the adjacent oxygen species around cerium sites as the active sites

Table 3 The surface atomic concentration of catalysts from XPS

	Surface atomic concentration						
Samples	W	Nb	Ce	Ce^{3+}/Ce	Zr	O	O_{ads}/O
10W/CZ	2.09	—	19.0	20.9	5.60	73.31	36.38
5W–5Nb/CZ	1.51	2.96	18.98	30.53	5.75	70.80	46.96
10Nb/CZ	—	3.78	22.66	25.09	5.82	67.74	30.73

possessed facile redox cycle between Ce^{4+} and Ce^{3+}, thereby, the reducibility of these cerium sites was modified and finally the reactivity of NH_3-SCR reaction was promoted over 5W–5Nb/CZ rather than 10W/CZ.

3.3 Redox properties

3.3.1 H_2-TPR. Fig. 8 displayed the H_2-TPR profiles of 10W/CZ, Nb-substituted W/CZ and 10Nb/CZ to investigate the effect of the substitution of WO_3 by Nb_2O_5 on the reducibility of the catalysts. H_2 consumptions of different reduction peaks were calculated by fitting the curves (shown in Fig. S3†) and adopting CuO as the standard sample. And the results were listed in Table 4. 10W/CZ presented two reduction peaks centered at 545 and 633 °C, which could be ascribed to the reduction of the surface active oxygen species and the lattice oxygen species, respectively, as reported in our previous work.[16] In terms of Nb-containing catalysts, Peak 1 and Peak 2 (listed in Table 4) were assigned to the reduction of the surface oxygen species, Peak 3 could be attributed to the reduction of oxygen of ceria from the carrier, Peak 4 at the high-temperature was ascribed to the lattice oxygen species.[36] Obviously, the redox properties of 10W/CZ were modified by the substitution of Nb_2O_5, as seen from Fig. 8. The temperatures of the reduction peaks were clearly transferred towards lower values after WO_3 was partially substituted by Nb_2O_5. Moreover, the onset reduction temperature of the active oxygen species was decreased from 392 °C of 10W/CZ to 278 °C of 5W–5Nb/CZ, further increasing the substitution amount of WO_3 by Nb_2O_5, it was shifted to higher

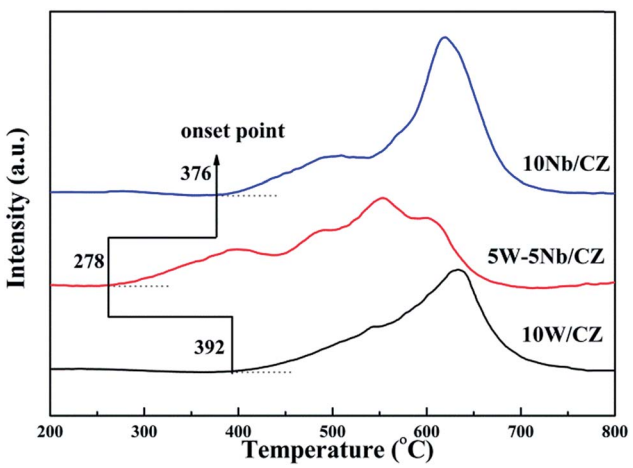

Fig. 8 H_2-TPR profiles of 10W/CZ 5W–5Nb/CZ and 10Nb/CZ.

Table 4 H_2 consumption and onset temperature of reduction peaks of different catalysts

	Peak 1		Peak 2		Peak 3		Peak 4	
Samples	T_m (°C)	H_2 consumption (μmol g^{-1})	T_m (°C)	H_2 consumption (μmol g^{-1})	T_m (°C)	H_2 consumption (μmol g^{-1})	T_m (°C)	H_2 consumption (μmol g^{-1})
10W/CZ	545	247.6	—	—	—	—	622	493.3
5W–5Nb/CZ	395	186.9	490	122.4	549	180.2	602	167.3
10Nb/CZ	490	220.7	—	—	535	82.3	592	587.6

temperature ranges. It meant that the reducibility of 10W/CZ was significantly improved by partial substitution of WO_3 with Nb_2O_5, thus, more facile reduction of active oxygen species was occurred at lower temperature range over 5W–5Nb/CZ rather than other investigated catalysts.[19] As summarized in Table 2, considering the similar surface area among the investigated catalysts, the H_2 consumption of active oxygen species was the largest on 5W–5Nb/CZ than other catalysts, which was consistent with the results of XPS O 1s and well in line with the NO oxidation activity as shown in Fig. 2. It could imply that the possible interaction existed between Ce^{n+} and Nb^{n+} over the catalysts with the coexistence of W and Nb. According to the ref. 37, the active oxygen species were readily available to take part in NH_3-SCR reaction at low-temperature ranges, which was related well with the concentration of NO_2 derived from the oxidation reaction of NO between active oxygen species. Therefore, the increase of reducibility and active oxygen species could be one of reasons that 5W–5Nb/CZ possessed the best low-temperature NH_3-SCR activity from Fig. 1a.

3.3.2 O_2-TPD. O_2-TPD measurements were carried out to further illustrate the enhancement of active oxygen species by appropriate substitution of WO_3 with Nb_2O_5 in 10W/CZ, and the results were presented in Fig. 9. According to the previous reports,[14,38] the desorption peak centered at below 350 °C could be ascribed to the active oxygen species (O_2 and O^-), the desorption peak corresponding to the lattice oxygen species (O^{2-}) was often located at above 750 °C, and the desorption peak between 350–750 °C could be mainly attributed to the oxygen vacancies. Accordingly, the main peaks of all investigated catalysts at about 150 °C were assigned to the active oxygen species from Fig. 9. It could be distinctly observed that 5W–5Nb/CZ possessed the lowest onset temperature and the largest desorption amount of active oxygen species than 10W/CZ and 10Nb/CZ. It indicated that the partial substitution amount of WO_3 by Nb_2O_5 indeed affected the availability of active oxygen species, and the above results were in agreement with the results of XPS and H_2-TPR. Therefore, the increased amount of active oxygen species could be reasonably ascribed to the interaction between Ce^{n+} and Nb^{n+}.[19]

3.4 Surface acidity

3.4.1 NH_3-TPD. NH_3-TPD was employed to estimate the effect of partial substitution of WO_3 by Nb_2O_5 on the surface acidities of 10W/CZ, and the curves were presented in Fig. 10. Below 450 °C, the curve shapes of 10W/CZ, 5W–5Nb/CZ and 10Nb/CZ were similar as each other from Fig. 10, in addition, the intensity of the desorption peak was increased in the followed sequence: 10Nb/CZ < 10W/CZ < 5W–5Nb/CZ. It could illustrate that the possible electronic interactions between W^{n+} and Nb^{n+} resulted in the enhancement of weak acid over 5W–5Nb/CZ. An obvious desorption peak centered at about 580 °C was observed over 10W/CZ, the corresponded peak intensity of 5W–5Nb/CZ was far lower than that of 10W/CZ, but no peaks

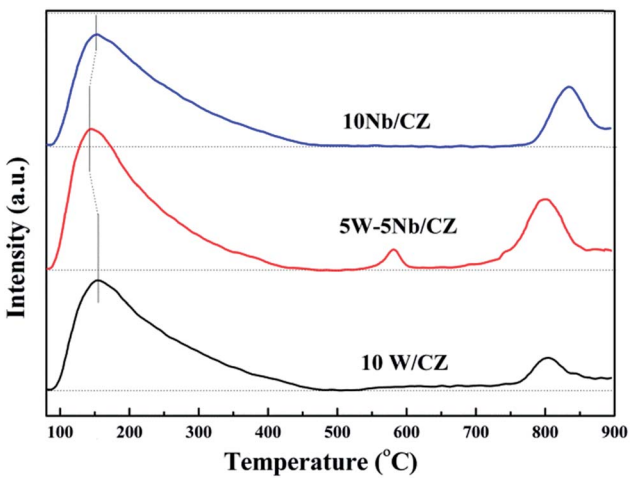

Fig. 9 O_2-TPD curves of 10W/CZ, 5W–5Nb/CZ and 10Nb/CZ.

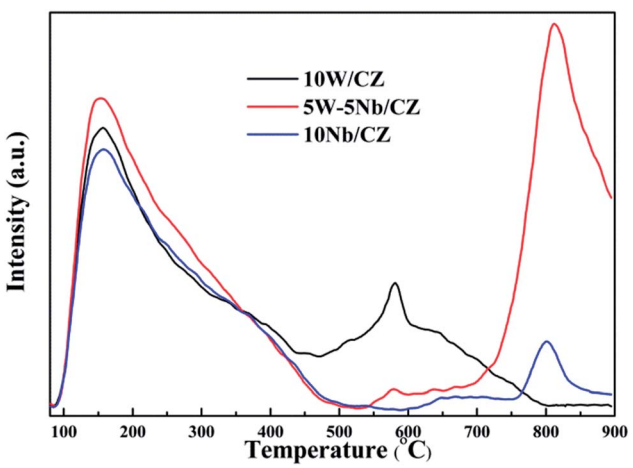

Fig. 10 NH_3-TPD curves of 10W/CZ, 5W–5Nb/CZ and 10Nb/CZ catalysts.

could be detected at the same temperature over 10Nb/CZ. It indicated that the desorption peak could be attributed to the medium Lewis acid sites from W=O of amorphous WO_3.[31] Moreover, the desorption peaks of NH_3 at about 800 °C were both observed over 5W–5Nb/CZ and 10Nb/CZ, and the peak intensity of the former was evidently higher than that of the later, no NH_3 was desorbed over 10W/CZ at above 800 °C. So the desorption peak might be assigned to strong acid derived from Nb_2O_5. The above phenomena indicated that 5W–5Nb/CZ inherited the acidities of 10W/CZ and 10Nb/CZ due to the possible electronic interactions between W and Nb. As seen from Fig. 10, it was obvious that the total peak area of catalysts followed the decreased sequence of 5W–5Nb/CZ > 10W/CZ > 10Nb/CZ, which suggested that the total surface acidity was evidently improved by partial substitution of WO_3 with Nb_2O_5 in 10W/CZ.

3.4.2 *In situ* DRIFTS of NH_3 adsorption. *In situ* DRIFTS of NH_3 adsorption was performed to investigate the influence of partial substitution of WO_3 with Nb_2O_5 on the acid type of 10W/CZ. Fig. 11 showed the *in situ* DRIFTS of NH_3 derived species over 10W/CZ, 5W–5Nb/CZ and 10Nb/CZ coming from adsorption of NH_3 at 200 °C in the wavenumber ranges of 4000–3000 and 2100–1000 cm^{-1}. The bands in the ranges of 1120–1239, 1580–1595 and 3164–3357 cm^{-1} attributed to the coordinated NH_3 and the bands at 1323–1335 cm^{-1} ascribed to NH_2 species were both bonded to the Lewis acid sites.[15,21,39] While the bands were corresponded to NH_4^+ species coordinated to Brønsted acid sites in the wavenumbers ranges of 1420–1440 and 1664–1670 cm^{-1}.[40,41] It could be seen that the intensities of bands ascribed to all acid sites were increased in the sequence of 5W–5Nb/CZ > 10W/CZ > 10Nb/CZ. From Fig. 11a, the negative bands at around 3680 and 3780 cm^{-1} could be attributed to the consumption of surface OH^- group by NH_3 to form NH_4^+.[42] The detailed ratios (B/L) of the integrated band areas of 1191–1239 and 1420–1440 cm^{-1}, which could be considered as the characteristic peaks for NH_3 and NH_4^+ species assigned to Lewis and Brønsted acid sites, were summarized in Fig. 11a. It was clear that the partial substitution of WO_3 by Nb_2O_5 in 10W/CZ evidently affected the distribution of acid sites over the surface of catalysts. The ratio of B/L was gradually enhanced with increasing the substitution amount of Nb_2O_5, suggesting the close relationship between acid sites and the content of NbO_x species, which was in accordance with the increased amount of Brønsted acid sites by partial substitution of WO_3 by Nb_2O_5 mentioned in Raman. Moreover, it should be noted that the negative bands at about 1984–1997 cm^{-1} could be only observed at 5W–5Nb/CZ and 10Nb/CZ. The above bands could be assigned to the stretching mode of Nb=O in the overtone region due to the overlap of the above stretching mode in the fundamental region (at about 980 cm^{-1}).[29] According to the ref. 21 the negative Nb=O at the overtone region implied that the bonds of Nb=O were consumed during the process of NH_3 adsorption. In other words, the bond of Nb=O could be a kind of acid sites for NH_3 adsorption.

The bonds of Nb=O could act as either Lewis acid sites or Brønsted acid sites in the literatures.[18,43] 5W–5Nb/CZ was selected as a sample to illustrate the role of Nb=O bonds during the process of NH_3 adsorption and investigate the behaviours of NH_3 adsorption in the temperature ranges of 50–350 °C, the results were presented in Fig. 11b. As mentioned above, the bands at 1234 and 1448 cm^{-1} could be considered as characteristic bands of Lewis and Brønsted acid sites, respectively, the negative bands at around 1984 cm^{-1} was ascribed to Nb=O overtones. It could be seen that the stability of Brønsted acid sites was lower than that of Lewis acid sites, because the intensity of bands at 1448 cm^{-1} depressed quickly with the enhancement of temperatures and completely disappeared at 300 °C from Fig. 11b. Meanwhile, the intensities of the bands at around 1234 cm^{-1} and the negative ones at 1984 cm^{-1} declined and vanished simultaneously, they basically disappeared at 350 °C, suggesting that the bonds of Nb=O could play the role as Lewis acid sites in this work. Furthermore, the negative bands at 3664 and 3756 cm^{-1} attributed to the surface OH^- groups, which were vanished simultaneously as the bands at 1448 cm^{-1} at 300 °C, were responsible for Brønsted acid sites.[21] Therefore, combined the above analysis, the desorption peak of NH_3 at about 150 °C should be attributed to weak Lewis and

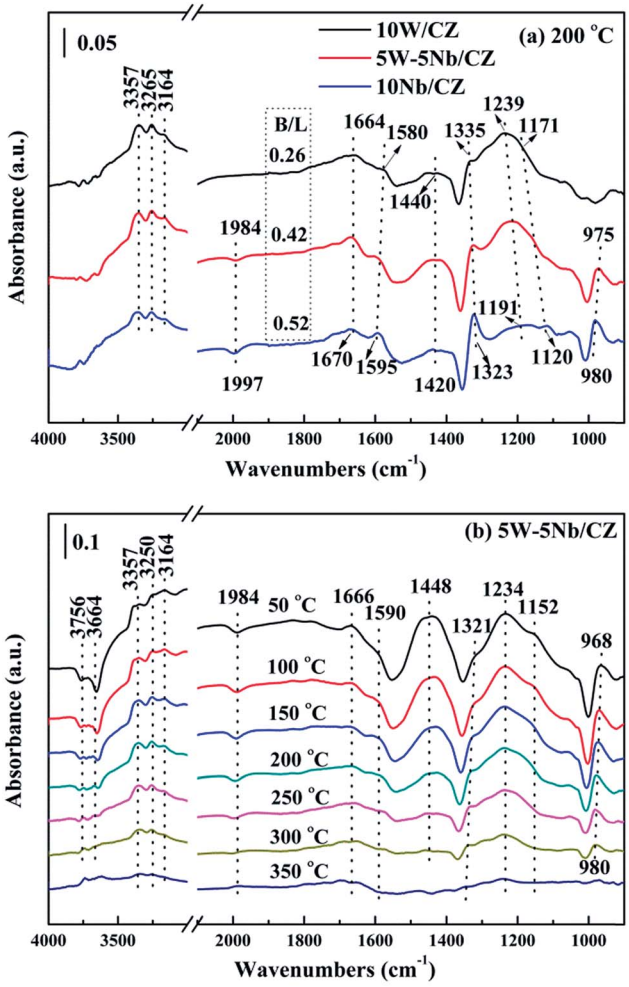

Fig. 11 *In situ* DRIFT spectra of 500 ppm NH_3 adsorption with 300 mL min^{-1} flow rate over the 10W/CZ, 5W–5Nb/CZ and 10Nb/CZ catalysts at 200 °C (a) and over 5W–5Nb/CZ at different temperatures (b).

Brønsted acid sites, and the increased weak acid over 5W–5Nb/CZ could be Brønsted acid sites from Nb–OH in Fig. 10. While the desorption peak at about 800 °C could be assigned to strong Lewis acid sites derived from Nb_2O_5 promoted by the possible electronic interaction between W^{n+} and Nb^{n+}.[40]

Based on the above analyses about the role of the acid sites, it could be declared that Lewis and Brønsted acid sites were together participated in the NH_3-SCR reaction.[44,45] The thermal stability of Brønsted acid sites was less than that of Lewis acid sites due to the vanish of the former at 300 °C from Fig. 11b, implying that Brønsted acid sites could mainly take part in the reaction in the relatively low temperature ranges.[31] However, the bands at 1234 cm^{-1} assigned to Lewis acid sites still could be observed at 350 °C, which meant that the Lewis acid sites might contribute to the NH_3-SCR reaction at the whole operation temperature range over 5W–5Nb/CZ. Consequently, WO_3 partial substitution by Nb_2O_5 in 10W/CZ resulted in an evident improvement of the total acidity of the catalyst, both Lewis and Brønsted acid sites could be supplied by Nb_2O_5, even though the total acidity of 10Nb/CZ was the smallest in the three catalysts. Therefore, compared with 10W/CZ, the increment of Brønsted acid sites by the substitution of Nb_2O_5 could be one of reasons that significantly improving $deNO_x$ activity below 250 °C over 5W–5Nb/CZ, in contrast, the enhancement of Lewis acid sites could not inhibit a slight decline of NO_x conversion due to the formation of NO_x from non-selective oxidation of NH_3 (in Fig. 3b and c) over 5W–5Nb/CZ in the high-temperature ranges.

4 Discussion

Analysis of the structure of catalysts from XRD and Raman, no obvious evidence of Nb_2O_5 over the catalysts with less than 5 wt% Nb_2O_5 indicated that niobium was as dispersed species over the surface of catalysts, while clear diffraction peak attributed to hexagonal Nb_2O_5 was detected over the catalysts with above 5 wt% Nb_2O_5. In addition, no diffraction peak ascribed to WO_3 phase over all catalysts was supported by XRD and Raman, indicating that WO_3 species were also dispersed over the surface of catalysts. The structural information from Raman, niobium oxides species with tetrahedral [NbO_4] structure were only observed over the catalysts with low loading of Nb_2O_5 ($\leq$5 wt%), since the [NbO_4] structure with four oxygen atoms surrounding Nb represented monomeric dispersion. The polymeric niobium oxide species with octahedral [NbO_x] structure was gradually formed and became to be the dominant structure by linking the isolated [NbO_4] units with the bridging oxygen, with increasing the content of Nb_2O_5. It meant that the polymeric or bulk NbO_x could be formed when the loading of Nb_2O_5 outstripped the monolayer coverage amount, which was supported by the results of XRD and Raman and was also in accordance with the literatures.[19,29] Also, the symmetrical W=O stretching mode assigned to the amorphous WO_3 species was detected by Raman of all W-containing catalysts except 3W–7Nb/CZ, suggesting the formation of a monolayer of WO_3 over the above catalysts.[30,31] According to the results of NH_3-TPD and *in situ* DRIFTS of NH_3, the decrease of medium Lewis acid sites for 5W–5Nb/CZ was closely related with the W=O bonds in WO_x species due to the decreased amount of WO_3, compared to 10W/CZ. Moreover, the increased strong Lewis acid sites and Brønsted acid sites were associated with Nb=O and Nb–OH, which has been confirmed the relationships with monolayer NbO_x species by the previous studies.[19,43] Based on the analysis of *in situ* DRIFTS of NH_3, Brønsted acid sites could be mainly participated in the relative low-temperature NH_3-SCR reaction due to its lower thermal stability than Lewis acid sites, accordingly, Lewis acid sites could take part in the whole operation temperature range of SCR reaction over W–Nb/CZ serial catalysts. Consequently, 5W–5Nb/CZ should achieve the best low-temperature and high-temperature $deNO_x$ activity than single W or Nb-containing catalysts in Fig. 1a, because the former possessed more Brønsted and Lewis acid sites than other two catalysts; but it should be noted that the high-temperature NO_x conversion (above 400 °C) over 5W–5Nb/CZ was obviously lower than that over 10W/CZ, under the condition of the former with far more Lewis acid sites (could inhibit the non-selective oxidation of NH_3 in the high-temperature range) than the later. It indicated that the acidity was not the only factor affected the $deNO_x$ activity over 5W–5Nb/CZ, in case the acid sites were sufficient. Therefore, the relationship between the redox properties and the NH_3-SCR performance should be discussed hereon.

The results of XRD approved that Nb^{n+} would be incorporated into the lattice of CZ due to smaller radius of Nb^{5+} than those of Ce^{4+} and Zr^{4+}. Compared with 10W/CZ, for W–Nb/CZ catalysts, the partial substitution of Ce^{4+}/Zr^{4+} in CZ lattice by Nb^{5+} could bring excess electron compensation by the generation of Ce^{3+}. UV-vis result indicated that 5W–5Nb/CZ, with the most excess electron derived from the strongest electronic interaction between Nb^{5+} and Ce^{4+} than other catalysts, possessed the most Ce^{3+} ions, which has been evidenced by the result of XPS. Ce^{3+} could lead to the charge imbalance and unsaturated chemical bonds, which was important to the formation of oxygen vacancies and less bonded oxygen.[24,35] It meant that the contiguous oxygen species around Ce^{n+} sites were activated by niobium. It was well known that cerium sites as active sites due to the facile redox cycle between Ce^{4+} and Ce^{3+}, could improve the reducibility of these cerium sites and thereby promote the NH_3-SCR activity of Ce-based catalysts.[13,21,35] The electronic interaction between Ce^{n+} and Nb^{n+} has been evidenced by the results of H_2-TPR and O_2-TPD. It has been reported that the low-temperature NH_3-SCR activity was governed by the redox properties of catalysts.[46,47] The amount of active oxides directly affected the redox property and thereby controlled the low-temperature $deNO_x$ activity, since the active oxygen species would be firstly consumed to carry out NH_3-SCR reaction. 5W–5Nb/CZ achieved the highest low-temperature NO_x conversion among the investigated catalysts, which was similar to its most active oxygen species in XPS, H_2-TPR and O_2-TPD. It indeed indicated that the amount of active oxygen species significantly affected the low-temperature $deNO_x$ activity. Moreover, the activity of NO oxidation over different catalysts followed the sequence of 5W–5Nb/CZ > 10Nb/CZ > 10W/CZ, which illustrated that the low-temperature activity was possibly improved by generating more NO_2 due to more active

oxygen species.[41,48] However, the promoted oxidation ability of NH_3 resulted in the peroxidation of NH_3 to form more NO and NO_2 (in Fig. 3b and c), and further led to the depressed high-temperature NO_x conversion of 5W–5Nb/CZ. It showed that the constraint existed between the redox property and surface acidity over 5W–5Nb/CZ, even though it possessed the strongest redox property and largest amount of surface acid sites.

Although Lietti *et al.*[47,49] has proposed that the low-temperature deNO_x activity was governed by the redox properties of catalysts, whereas the high-temperature NO_x conversion was controlled by the acid sites over the surface of catalysts. And Dong *et al.*[8] suggested that the adequate acid sites initiated the NH_3-SCR reaction and the redox ability of catalysts could upgrade the SCR activity. Based on the above analysis, it is reasonable that the balance should occur between the surface acidity and redox property over catalysts and then could achieve the optimal NH_3-SCR performance both in low and high temperatures ranges. Therefore, it is necessary to investigate the balance between surface acidity and redox property over Nb-substituted W/CZ catalysts and the related work is under way.

5 Conclusions

A series of Nb substituted W/CZ catalysts, prepared by co-impregnated methods, displayed excellent deNO_x activity and N_2 selectivity. Among them, 5W–5Nb/CZ with the substitution of 5 wt% WO_3 by 5 wt% Nb_2O_5 achieved above 90% NO_x conversion in a broad reaction temperature window of 190–434 °C and nearly 100% N_2 selectivity within the whole operation temperature range. The characterization results demonstrated that 5W–5Nb/CZ possessed more Brønsted acid sites from the substituted NbO_x and stronger redox property due to more Ce^{3+}, oxygen vacancies and active oxygen species than other catalysts, which could contribute to its best low-temperature (below 250 °C) NO_x conversion. The high-temperature (above 400 °C) deNO_x activity of 5W–5Nb/CZ was lower than that of 10W/CZ, in case that the former possessed more Lewis acid sites than the latter, which could be resulted from the formation of NO_x from the peroxidation of NH_3 in the high temperatures over 5W–5Nb/CZ with stronger redox property than 10W/CZ. Therefore, the constraint between the redox property and surface acidity could prevent the optimal NH_3-SCR performance over 5W–5Nb/CZ in the whole operation temperature range, and the investigation on the balance between the redox property and surface acidity is under way.

Conflicts of interest

There are no conflicts to declare.

Acknowledgements

This work was financially supported by the National High-Tech Research and Development (863) Program of China (Grant 2015AA034603) and the Science and Technology Project of Chengdu City (Grant 2015-HM01-00475-SF).

References

1 S. Roy, M. S. Hegde and G. Madras, *Appl. Energy*, 2009, **86**, 2283–2297.
2 T. Boningari and P. G. Smirniotis, *Curr. Opin. Chem. Eng.*, 2016, **13**, 133–141.
3 K. Skalska, J. S. Miller and S. Ledakowicz, *Sci. Total Environ.*, 2010, **408**, 3976–3989.
4 F. Liu, Y. Yu and H. He, *Chem. Commun.*, 2014, **50**, 8445–8463.
5 P. G. Smirniotis, D. A. Peña and B. S. Uphade, *Angew. Chem., Int. Ed.*, 2001, **40**, 2479–2482.
6 S. S. R. Putluru, L. Schill, A. Godiksen, R. Poreddy, S. Mossin, A. D. Jensen and R. Fehrmann, *Appl. Catal., B*, 2016, **183**, 282–290.
7 M. Haneda, T. Morita, Y. Nagao, Y. Kintaichi and H. Hamada, *Phys. Chem. Chem. Phys.*, 2001, **3**, 4696–4700.
8 C. Tang, H. Zhang and L. Dong, *Catal. Sci. Technol.*, 2016, **6**, 1248–1264.
9 Y. Li, H. Cheng, D. Li, Y. Qin, Y. Xie and S. Wang, *Chem. Commun.*, 2008, **12**, 1470–1472.
10 P. Ning, Z. Song, H. Li, Q. Zhang, X. Liu, J. Zhang, X. Tang and Z. Huang, *Appl. Surf. Sci.*, 2015, **332**, 130–137.
11 F. Can, S. Berland, S. Royer, X. Courtois and D. Duprez, *ACS Catal.*, 2013, **3**, 1120–1132.
12 A. Väliheikki, T. Kolli, M. Huuhtanen, T. Maunula and R. L. Keiski, *Top. Catal.*, 2015, **58**, 1002–1011.
13 H. Xu, Y. Cao, Y. Wang, Z. Fang, T. Lin, M. Gong and Y. Chen, *Chin. Sci. Bull.*, 2014, **59**, 3956–3965.
14 H. Xu, Y. Li, B. Xu, Y. Cao, X. Feng, M. Sun, M. Gong and Y. Chen, *J. Ind. Eng. Chem.*, 2016, **36**, 334–345.
15 H. Xu, M. Sun, S. Liu, Y. Li, J. Wang and Y. Chen, *RSC Adv.*, 2017, **7**, 24177–24187.
16 H. Xu, X. Feng, S. Liu, Y. Wang, M. Sun, J. Wang and Y. Chen, *Appl. Surf. Sci.*, 2017, **419**, 697–707.
17 S. Shwan, R. Nedyalkova, J. Jansson, J. Korsgren, L. Olsson and M. Skoglundh, *Ind. Eng. Chem. Res.*, 2012, **51**, 12762–12772.
18 I. Nowak and M. Ziolek, *Chem. Rev.*, 1999, **99**, 3603–3624.
19 Z. Ma, X. Wu, Z. Si, D. Weng, J. Ma and T. Xu, *Appl. Catal., B*, 2015, **179**, 380–394.
20 M. Casapu, O. Kröcher, M. Mehring, M. Nachtegaal, C. Borca, M. Harfouche and D. Grolimund, *J. Phys. Chem. C*, 2010, **114**, 9791–9801.
21 R. Qu, X. Gao, K. Cen and J. Li, *Appl. Catal., B*, 2013, **142**, 290–297.
22 S. Ding, F. Liu, X. Shi and H. He, *Appl. Catal., B*, 2016, **180**, 766–774.
23 M. Casapu, A. Berhard, D. Peitz, M. Mehring, M. Elsener and O. Kröcher, *Appl. Catal., B*, 2011, **103**, 79–84.
24 H. Xu, Y. Wang, Y. Cao, Z. Fang, T. Lin, M. Gong and Y. Chen, *Chem. Eng. J.*, 2014, **240**, 62–73.
25 Y. Cui, R. Fang, H. Shang, Z. Shi, M. Gong and Y. Chen, *J. Alloys Compd.*, 2015, **628**, 213–221.
26 I. Kosacki, T. Suzuki, H. U. Anderson and P. Colomban, *Solid State Ionics*, 2002, **149**, 99–105.

27 B. M. Reddy and A. Khan, *Langmuir*, 2003, **19**, 3025–3030.
28 M. A. Bañares and I. E. Wachs, *J. Raman Spectrosc.*, 2002, **33**, 359–380.
29 L. J. Burcham, J. Datka and I. E. Wachs, *J. Phys. Chem. B*, 1999, **103**, 6015–6024.
30 X. Li, M. Shen, X. Hong, H. Zhu, F. Gao, Y. Kong, L. Dong and Y. Chen, *J. Phys. Chem. B*, 2005, **109**, 3949–3955.
31 Y. Peng, K. Li and J. Li, *Appl. Catal., B*, 2013, **140–141**, 483–492.
32 S. Tsunekawa, T. Fukuda and A. Kasuya, *J. Appl. Phys.*, 2000, **87**, 1318–1321.
33 J. Zhu, F. Gao, L. Dong, W. Yu, L. Qi, Z. Wang, L. Dong and Y. Chen, *Appl. Catal., B*, 2010, **95**, 144–152.
34 D. R. Sellick, A. Aranda, T. García, J. M. López, B. Solsona, A. M. Mastral, D. J. Morgan, A. F. Carley and S. H. Taylor, *Appl. Catal., B*, 2013, **132–133**, 98–106.
35 J. Yu, Z. Si, L. Chen, X. Wu and D. Weng, *Appl. Catal., B*, 2015, **163**, 223–232.
36 Z. Ma, D. Weng, X. Wu, Z. Si and B. Wang, *Catal. Commun.*, 2012, **27**, 97–100.
37 P. W. Seo, S. P. Cho, S. H. Hong and S. C. Hong, *Appl. Catal., A*, 2010, **380**, 21–27.
38 L. Zhu, J. Yu and X. Wang, *J. Hazard. Mater.*, 2007, **140**, 205–210.
39 Y. Peng, C. Liu, X. Zhang and J. Li, *Appl. Catal., B*, 2013, **140–141**, 276–282.
40 L. Zhang, L. Li, Y. Cao, Y. Xiong, S. Wu, J. Sun, C. Tang, F. Gao and L. Dong, *Catal. Sci. Technol.*, 2015, **5**, 2188–2196.
41 W. Shan, F. Liu, H. He, X. Shi and C. Zhang, *Appl. Catal., B*, 2012, **115–116**, 100–106.
42 F. Liu, K. Asakura, H. He, Y. Liu, W. Shan, X. Shi and C. Zhang, *Catal. Today*, 2011, **164**, 520–527.
43 T. Onfroy, G. Clet and M. Houalla, *J. Phys. Chem. B*, 2005, **109**, 14588–14594.
44 L. Chen, J. Li and M. Ge, *Environ. Sci. Technol.*, 2010, **44**, 9590–9596.
45 A. Vittadini, M. Casarin and A. Selloni, *J. Phys. Chem. B*, 2005, **109**, 1652–1655.
46 L. Lietti and P. Forzatti, *J. Catal.*, 1994, **147**, 241–249.
47 L. Lietti, J. L. Alemany, P. Forzatti, G. Busca, G. Ramis, E. GIamello and F. Bregani, *Catal. Today*, 1996, **29**, 143–148.
48 Y. Wei, J. Liu, Z. Zhao, A. Duan and G. Jiang, *J. Catal.*, 2012, **287**, 13–29.
49 L. Lietti, P. Forzatti and F. Berti, *Catal. Lett.*, 1996, **41**, 35–39.